NASA-CR-197488

ORIGINAL CONTAINS
COLOR ILLUSTRATIONS

Numerical Simulation of Helicopter Engine Plume in Forward Flight

Final Report Cooperative Agreement #NCC2-5061

FINAL
IN-02-CR
COLOR PLATES
33902
P-12

Arsenio C.B. Dimanlig
Cornelis P. van Dam
Dept. of Mechanical and Aeronautical Engineering
University of California, Davis

Earl P.N. Duque
US Army Aeroflightdynamics Directorate
NASA Ames Research Center

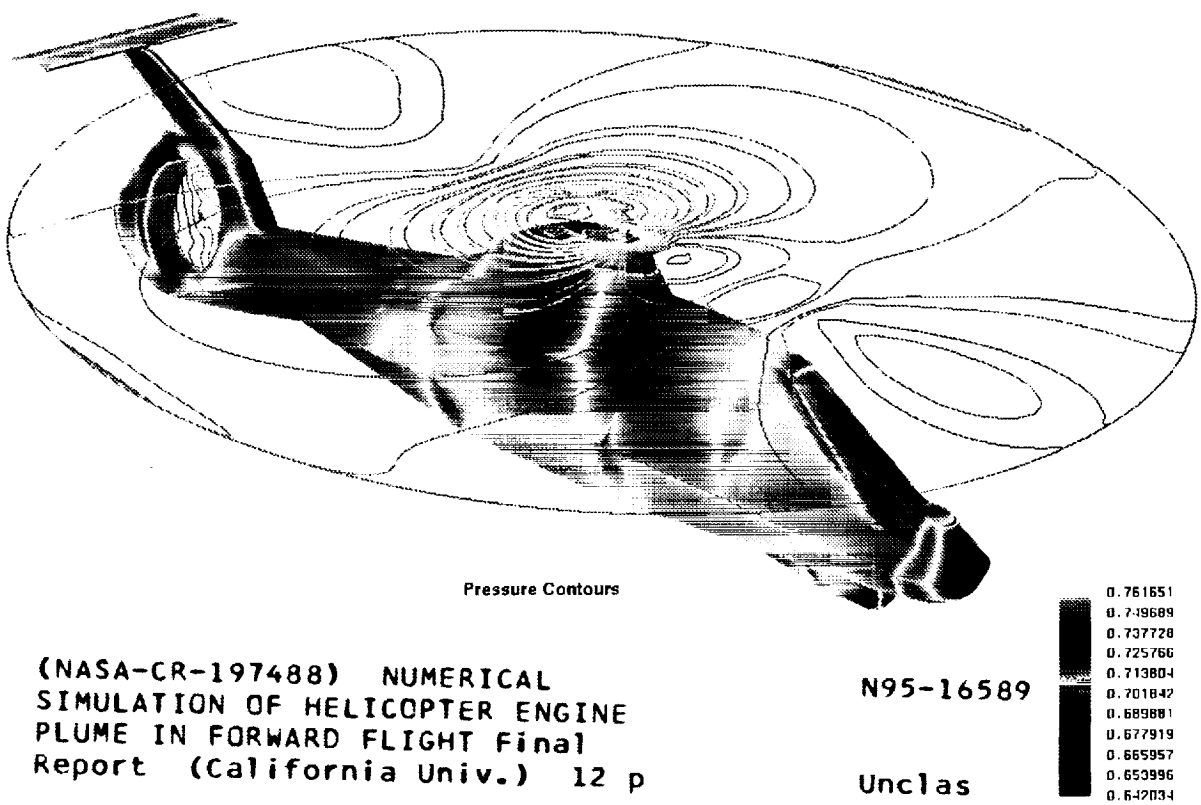

(NASA-CR-197488) NUMERICAL SIMULATION OF HELICOPTER ENGINE PLUME IN FORWARD FLIGHT Final Report (California Univ.) 12 p

N95-16589

Unclas

G3/02 0033902

Numerical Simulation of Helicopter Engine Plume in Forward Flight

Final Report Cooperative Agreement #NCC2-5061

Cornelius P. Van Dam
Arsenio C.B. Dimanlig
Dept of Mechanical and Aeronautical Engineering
University of California, Davis

Earl P.N. Duque
US Army Aeroflightdynamics Directorate
NASA Ames Research Center

1.0 Introduction

Flowfields around helicopters contain complex flow features such as large separated flow regions, vortices, shear layers, blown and suction surfaces and an inherently unsteady fulfilled imposed by the rotor system. Another complicated feature of helicopters are their infrared signature. Typically, the aircraft's exhaust plume interacts with the rotor downwash, the fuselage's complicated flowfield, and the fuselage itself giving each aircraft a unique IR signature at given flight conditions.

The goal of this project was to compute the flow about a realistic helicopter fuselage including the interaction of the engine air intakes and exhaust plume. The computations solve the Thin-Layer Navier Stokes equations using overset type grids and in particular use the OVERFLOW code by Buning [1] of NASA Ames. During this three month effort, an existing grid system of the Comanche Helicopter was to be modified to include the engine inlet and the hot engine exhaust. The engine exhaust was to be modeled as hot air exhaust. However, considerable changes in the fuselage geometry required a complete regriding of the surface and volume grids. The engine plume computations have been delayed to future efforts. The results of the current work consists of a complete regeneration of the surface and volume grids of the most recent Comanche fuselage along with a flowfield computation.

2.0 Grid Generation and Flow Solver

The surface grids, volume grids and flow solutions were all obtained using currently available codes either developed at NASA Ames or through contract. For the surface grids, the

PRECEDING PAGE BLANK NOT FILMED

ICEM-CFD [2] code was used to read and modify the CAD IGES files. The IGES files had lacked some very small regions so required repair. With the ICEM code the grids were properly embellished for the next step in the grid generation process. A majority of the surface grids were generated using either the S3D program by Luh et.al. [3] or the GRIDGEN2D program by Steinbrenner [4].

Once the surface grids were obtained, the three-dimensional hyperbolic grid generation program by Chan [5], HYPGEN, along with its graphics users interface, HGUI, were used to generate the volume grids. The system of overset grids were then connected using the PEGASUS 4.1 program by Suh's [6]. The next section describes in more details the surface and resulting volume grids.

The flow solver OVERFLOW 1.6al by Buning [1] was used. The OVERFLOW code has considerable advantages over other Thin-layer Naiver-Stokes codes. In particular it uses overset grids and allows for various types of boundary conditions. For complex configuration computations such as a complete helicopter, the flexibility of arbitrary boundary conditions along with the overset grids gives one much flexibility in grid generation. In addition, researchers within both the rotorcraft CFD group and within NASA have provided considerable support to this program. The grid generation tools mentioned above along with numerous other tools have been developed to support this program. Recently, the rotorcraft CFD group has been incorporating its most latest flow solver developments into the OVERFLOW code. These developments improve the stability limits for unsteady computations and allow for dynamic grid motions. These methods will allow for the eventual computation of the interaction between the rotor and fuselage.

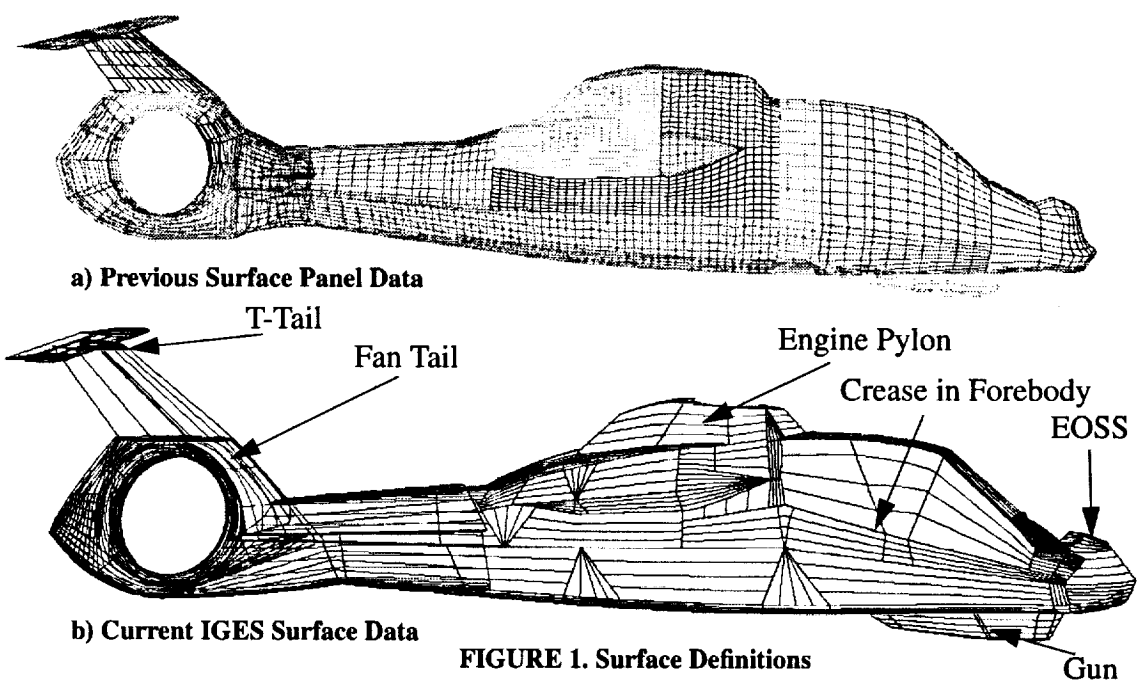

a) Previous Surface Panel Data

b) Current IGES Surface Data

FIGURE 1. Surface Definitions

3.0 Surface Grid Definition Changes

In a previous project, the surface grid, volume grids and solutions were obtained for the RAH-66 Comanche Helicopter. The project at that time was based upon the geometry provided by Sikorsky helicopters. Since then, the configuration has gone through some significant changes such as around the EOSS, the Fan-Tail, canopy regions, gun mount and engine pylon. This year we were provided with an CAD IGES definition that described the most recent fuselage lines.

Figure 1 compares the surface panel grids that were used to form the earlier surface grid and the current CAD IGES surface definitions. Figure 1b highlights the key differences between the two definitions. The forebody shape of the gun mount has a more square/faceted shape. The EOSS has a much more defined shape than before and more fully describes its multiply faceted surface. In addition, the EOSS grid is allowed to rotate the sensor to any position so that we can place it into any position and investigate its influence upon the flowfield. The fuselage forebody has a much more faceted shape and has better definition in the current dataset. The engine pylon has a different shape than originally defined. The Fan-tail has a more faceted shape than before so required regriding. Finally, the T-tail has a different definition. The horizontal tail fitted differently with the vertical tail and the vertical tail has a different taper and sweep than before.

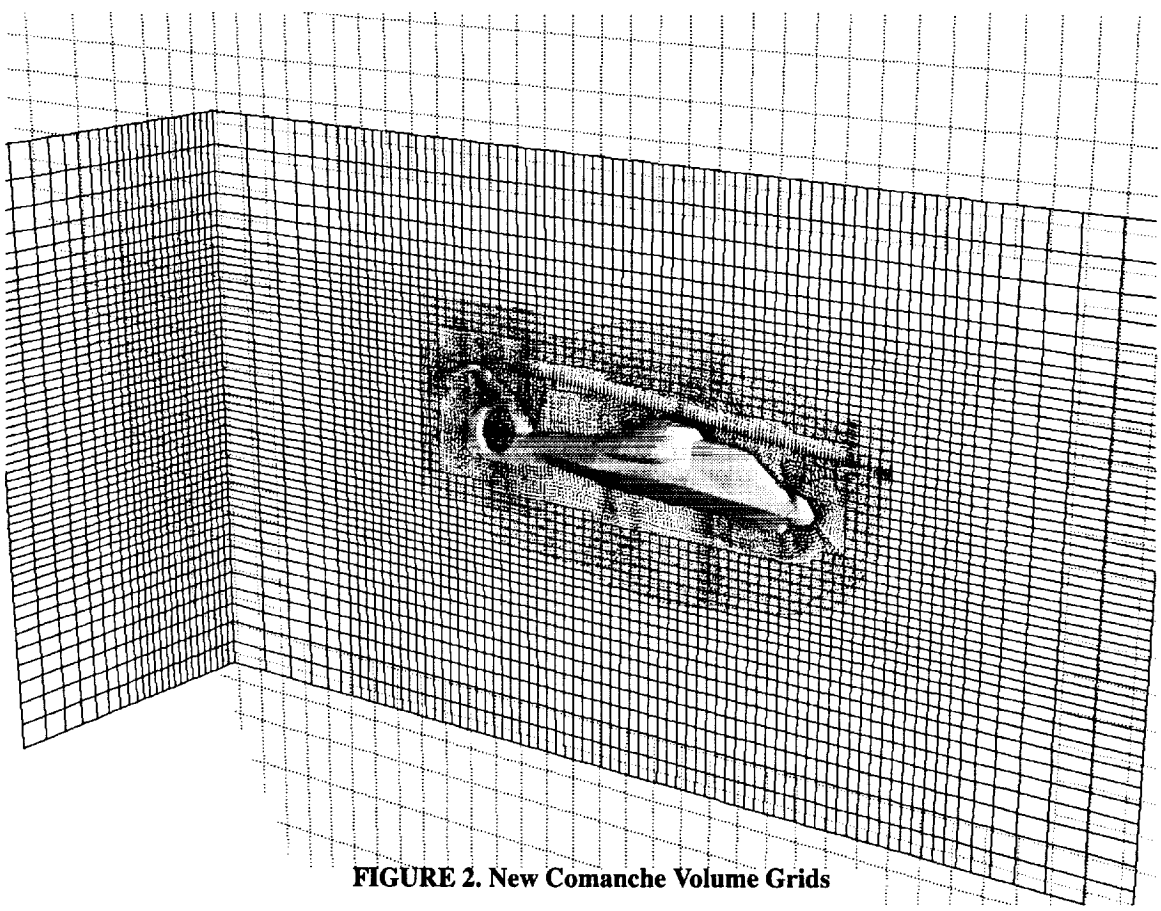

FIGURE 2. New Comanche Volume Grids

TABLE 1. Comanche Grid System

	Indices	Points
nose1	33x41x38	51414
nose2	50x59x33	97350
nose4	26x41x21	22386
canopy	69x131x40	361560
gun1	99x33x33	107811
gun2	51x11x33	18513
engine1	107x32x37	126688
engine2	61x181x40	441640
engine3	18x15x37	9990
back	55x131x40	288200
fan1	77x46x31	109802
fan2	75x21x34	53550
fan3	61x39x33	78507
finv	93x26x 35	84630
finhr	89x25x35	77875
finhl	89x25x35	77875
collar1	27x19x30	15390
collar2	25x20x30	15000
collar3	41x23x39	36777
collar4	24x24x30	17280
collar5	39x21x45	36855
collar6	45x21x34	32130
fintr	45x31x33	46035
fintl	45x31x33	46035
cube1	77x49x51	192423
cube2	58x73x99	419166
cube3	58x41x41	97498
fandisk	101x36x26	94536
actdisk5	151x51x50	385050
total		3441966

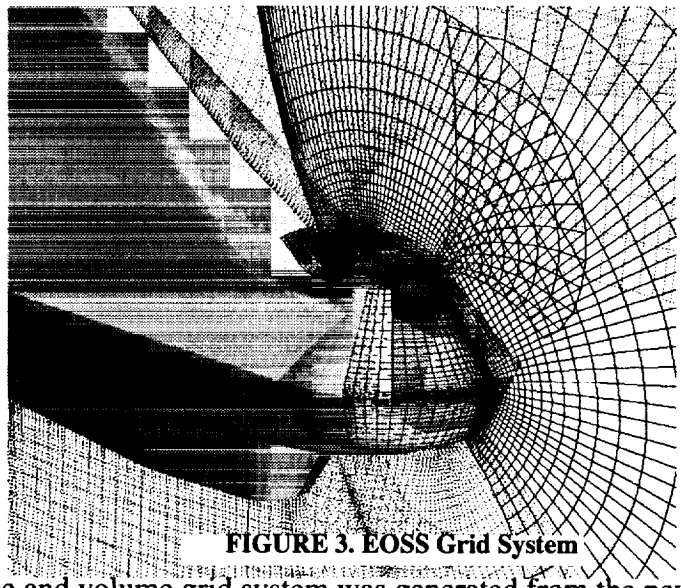

FIGURE 3. EOSS Grid System

A complete surface and volume grid system was generated from the new database. Figure 2 illustrates the entire grid volume grid system with the surface grids defined by the new surface grids. The complete grid system consists of 29 volume grids - 24 grids defined the fuselage itself with 3 Cartesian like meshes used to carry the solution to the farfield and facilitate connectivity between the individual grids and 2 actuators disk grids account for the rotor downwash and fan-tail. Table 1 highlights the grid point totals for each grid system.

Major subsections of the fuselage required a number of surfaces and volumes grids to adequately define the grids. Figure 3 illustrates the 3 grids that define the EOSS surface. The grid system was defined to allow the EOSS sensor to rotate to any position. By allowing this feature, the positioning influence upon the flow can be determined. The EOSS grid consists 171150 grid points with 3 overlapped grids

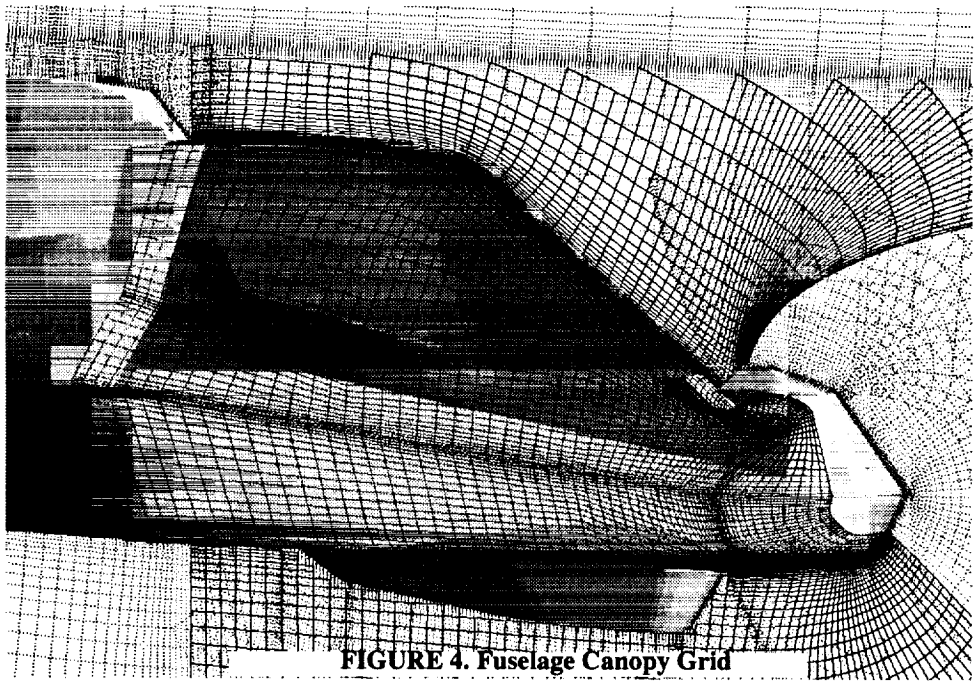

FIGURE 4. Fuselage Canopy Grid

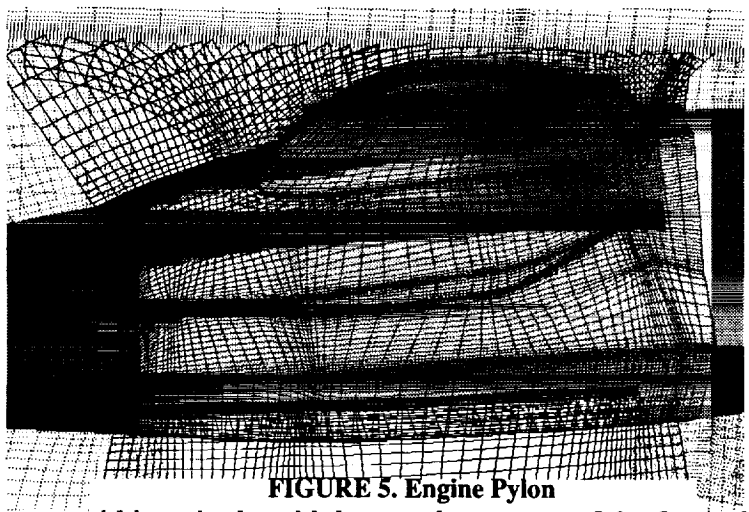

FIGURE 5. Engine Pylon

The fuselage canopy grid is a single grid that resolves many of the faceted surfaces and resulting crease lines in this important part of the fuselage. Figure 4 illustrates the resulting grid. As shown, the surface grid intersects with the EOSS grid system and the gun mount grid system. The volume grid intersects with the rotor grid above which results in hole points. The Canopy consists of 361,560 grid points.

The Engine pylon shown in Figure 5 had a number of changes. The upper part of the pylon was reshaped along with some changes in the engine inlet shapes. In addition, there was a change in the shape of the vortex generator (surfboard) that is mounted on top of the engine pylon between the pylon and the rotor hob fairing. The current grid system now better represents the most current fuselage lines

In the previous grid system, the T-Tail assembly did not include the vertical tail. One of the major goals for the current grid generation effort was to include the vertical tail. Figure 6 illustrates the resulting assembly. This grid system required 5 grids to properly define the horizontal tail and vertical tail. Four (4) collar type grids were used to attach the

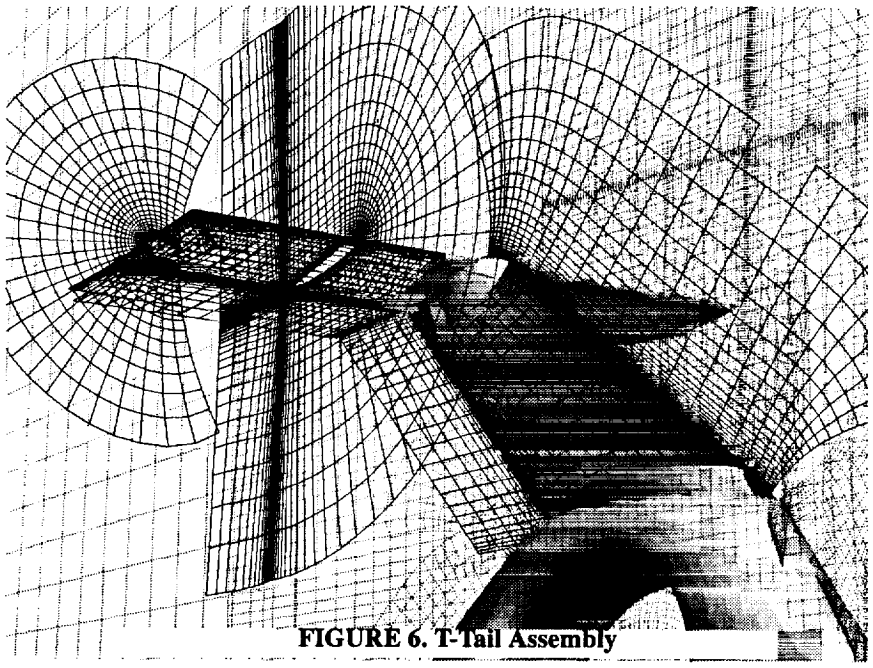

FIGURE 6. T-Tail Assembly

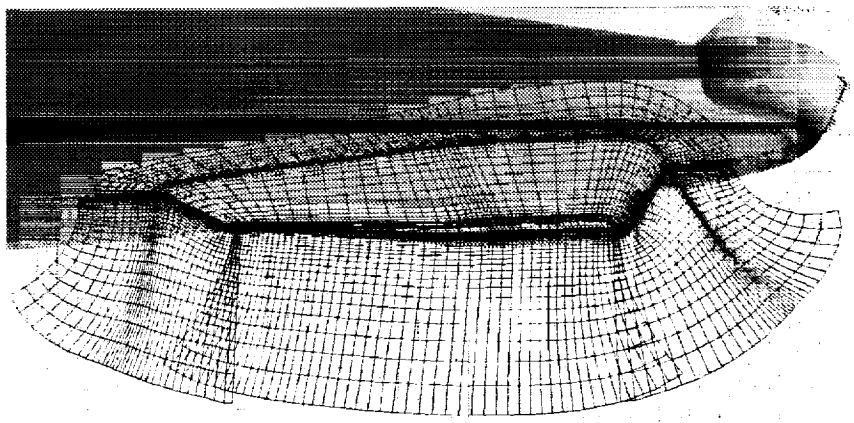

FIGURE 7. Engine Pylon

horizontal tail to the vertical tail while 2 collar grids were used to attach the vertical tail to the top of the fan-tail. The horizontail tail is a C-H topology over the major part of the tail with two tip caps that resolve the beveled shape of the tail. The vertical tail is also C-H topology. The grid system has a total of 727,741 grid points.

The gun mount has some major changes in shape and had to be regenerated. Figure 7 illustrates the new gun mount grid. The grid consists of 2 individual grids. It has a collar that fits it to the fuselage surface and a top cap grid that completes the configuration. The grid intersects primarily with the fuselage grid. Provision for gun turret placement is available with the current grid system.

4.0 Solution

A solution was obtained with the new surface and volume grids at a flow condition identical earlier computations. This new computation was designed to validate the computation against the previous computations and against planned wind tunnel tests. The flow field was set at an angle of attack of 0 degrees, free stream Mach number of 0.26 and Reynolds number based on fuselage length of 14,000,000. The actuator disks' constant pressure

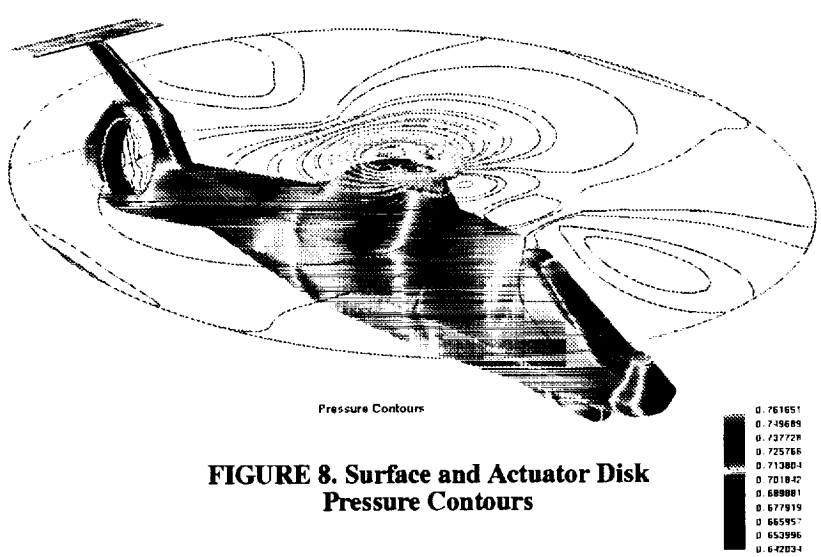

FIGURE 8. Surface and Actuator Disk Pressure Contours

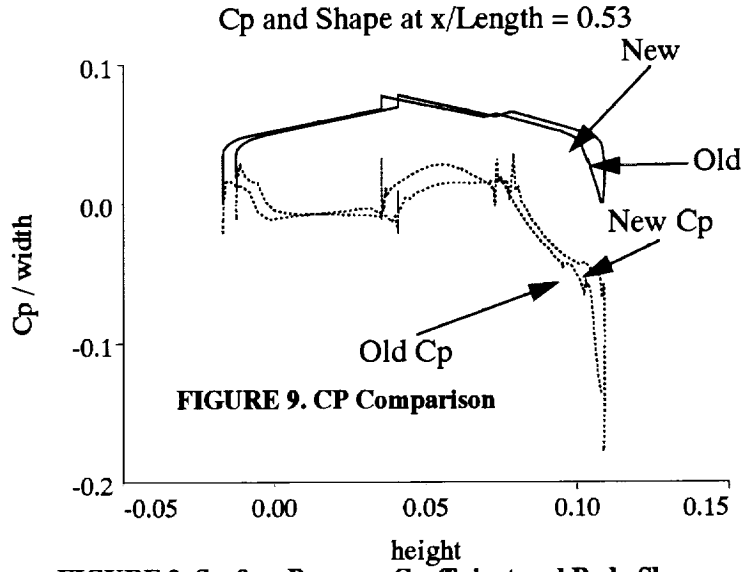

FIGURE 9. CP Comparison

FIGURE 9. Surface Pressure Coefficient and Body Shape

jump was based upon a rotor thrust coefficient of 0.009 for the fan and main rotor. The pressure jumps were based on a forward speed of 150 knots and tip Mach number of 0.65 at standard sea level.

Figure 8 illustrates the resulting surface pressure map and the actuator disk pressure contour maps. The solution shows much symmetry over most of the fuselage. However, asymmetry in the flow field becomes apparent towards the end of the tail boom where the geometry transitions from the fuselage to the fan-tail assembly. A comparison of the surface pressure at the location 0.53 fuselage lengths from the nose, Figure 9, shows that the

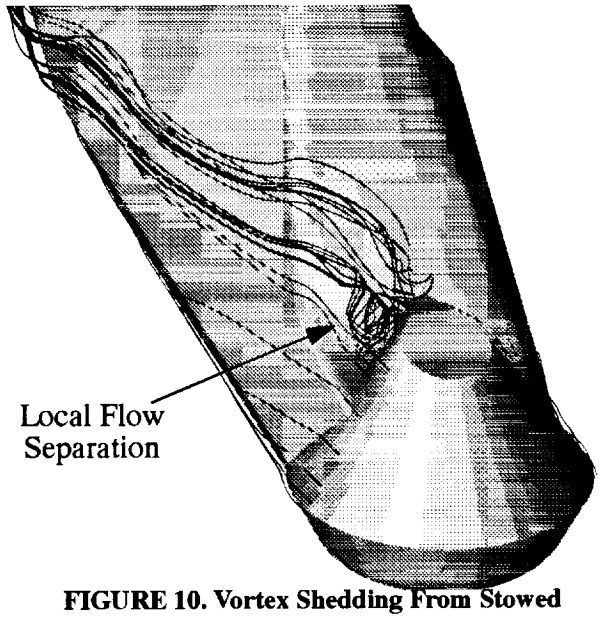

FIGURE 10. Vortex Shedding From Stowed

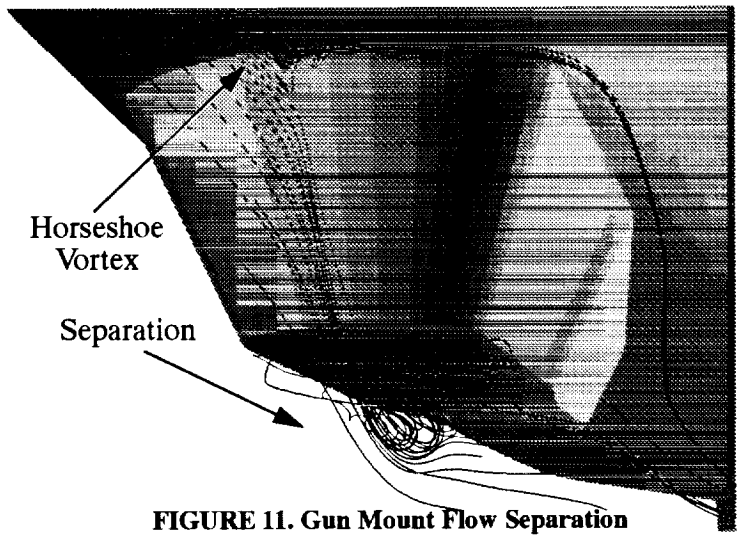

FIGURE 11. Gun Mount Flow Separation

solution has indeed changed due to the geometry changes. It also shows that the solution does not differ from the previous solution.

The solutions show some very different behavior as compared to the previous solution. One major difference is the apparent asymmetric unsteady flow caused by a wake from the EOSS. The unsteady wake generated by the EOSS strikes the fuselage canopy resulting in an unsteady load on the canopy. Figure 9 illustrates the vortex shedding and asymmetric flow at the EOSS through the use of particle traces. One should note the asymmetry in the flowfield. The green particle traces have been released from opposing grid locations but flow downstream in a non-symmetric way. The blue and read particles tend to wrap themselves into a separated region indicating flow separation.

The Comanche fuselages's faceted shape tends to cause numerous local flow separation areas. One of the significant areas is around the Gun mount and around the Fan-Tail. The gun mount exhibits a flow separation around the top leading edge of the mount. Figure 11 illustrates the flow separation. The green particle traces were release ahead of the mount along the symmetry plane. The red particle traces were released closer to the mount but also along the symmetry plane. The red and green particles flow into a horseshoe vortex at the joint between the fuselage canopy and the mount. At the upper part of the mount, the particles flow into a largely separated flowfield region. The separated flowfield on the upper part of the mount can have considerable effects on the aircraft performance and vibrations.

The Fan-tail exhibited some considerable flowfield separation as shown below in Figure 12. In this computation, the fan rotor was modeled using a constant pressure actuator disk with a pressure jump that effects a thrust coefficient of 0.009. Even with flow through the disk, the flowfield evidently separates which can become a considerable source of drag.

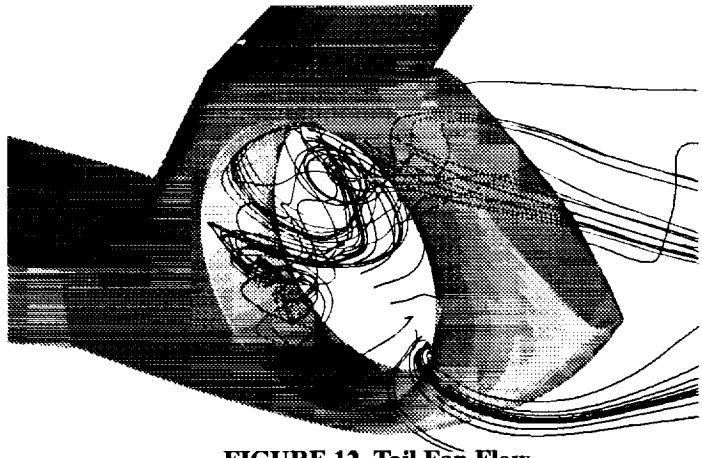

FIGURE 12. Tail Fan Flow

5.0 Summary and Recommendations

The flowfield about the latest RAH-66 Comanche helicopter fuselage definition was performed. The intended flowfield with engine exhaust and inlets were postponed because of the considerable changes with the fuselage definition. The effort shown in this report concentrated upon regriding the surface and volume grids to represent these most current lines of the aircraft. A grid system and flow solution were obtained. The solutions show some differences from earlier solutions. But the solutions do not vastly differ and give some confidence in the current solutions. This report highlighted a few regions of the aircraft and noted some regions of concern. Most notably the flow separations around the EOSS, gun mount and fan tail.

The flow solution still requires validation against experiment. Wind tunnel experiments by Berry at AFDD Langley will be carried out sometime in the early part of 1995. Computations of the isolated fuselage will be obtained at flowfield conditions that compare to the experiment. In addition, the Langley model will use a four bladed Comanche rotor. Unsteady flowfield measurements will be available. To support these experiments, a fuselage with rotor computation will be completed at flow conditions comparable to the experiment. Finally, engine inlet and exhaust analysis is still important. A future effort that continues the current project is recommended.

6.0 References

[1] Buning, P.G., Chiu, I.T., Obayashi, S., Rizk, Y.M., and Steger, J.L., "Numerical Simulation of the Integrated Space Shuttle Vehicle in Ascent,", AIAA 88-4359, August 1988.

[2] ICEM User's Manual, CDI Incorporated.

[3] Luh, R., "Surface Grid Generation for Complex Three-Dimensional Geometries" NASA Technical Memorandum 101046.

[4] Steinbrenner, J.P, Chawner, J.R. and Fouts, C.L., "The GRIDGEN 3-D Multiple Block Grid Generation System, User's Manual", WRDC-TR-90-3022, Wright Research and Development Center

[5] Chan, W.M. and Steger, J.L., Enhancements of a Three-Dimensional Hyperbolic Grid Generation Scheme, Applied Math and Comp., 51, 181-205, 1992.

[6] Suhs, N.E., and Tramel, R.E., PEGSUS 4.0 Users Manual, Arnold Engineering Development Center, AEDC-TR-91-8, June 1991.

[7] Dimanlig A.C.B, Hafez, M. and Duque E.P.N., " Numerical Simulation of Flow about Helicopter Fuselages, Final Report NCA2-789", October 15,1993.